INSTRUMENTATION AND MEASUREMENT

Measurements of Majorana transition frequency shift in caesium atomic fountain clocks

Jun-Ru Shi(施俊如)[1,2,3], Xin-Liang Wang(王心亮)[1,2,†], Fan Yang(杨帆)[1,2,3], Yang Bai(白杨)[1,2,3], Yong Guan(管勇)[1,2], Si-Chen Fan(范思晨)[1,2,3], Dan-Dan Liu(刘丹丹)[1,2], Jun Ruan(阮军)[1,2], and Shou-Gang Zhang(张首刚)[1,2]

[1] *National Time Service Center, Chinese Academy of Sciences, Xi'an* 710600, *China*
[2] *Key Laboratory of Time and Frequency Primary Standards, Chinese Academy of Sciences, Xi'an* 710600, *China*
[3] *University of Chinese Academy of Sciences, Beijing* 100049, *China*

(Received 28 March 2022; revised manuscript received 18 July 2022; accepted manuscript online 22 July 2022)

The caesium atomic fountain clock is a primary frequency standard. During its operation, a Majorana transition frequency shift will occur once a magnetic field at some special locations along the atomic trajectory is singular. In this study, by developing a physical model, we analyzed the magnetic field requirements for atomic adiabatic transition and calculated the influence of the Majorana atomic transition on the atomic state via a quantum method. Based on the simulation results for the magnetic field in the fountain clock, we applied the Monte Carlo method to simulate the relationship between the Majorana transition frequency shift and the magnetic field at the entrance of the magnetic shielding, as well as the initial atomic population. Measurement of the Majorana transition frequency shift was realized by state-selecting asymmetrically populated atoms. The relationship between the Majorana transition frequency shift and the axial magnetic field at the entrance of the magnetic shielding was obtained. The measured results were essentially consistent with the calculated results. Thus, the magnetic field at the entrance of the magnetic shielding was configured, and the Majorana transition frequency shift of the fountain clock was calculated to be 4.57×10^{-18}.

Keywords: caesium atomic fountain clock, Majorana transition frequency shift, magnetic field, initial atomic population

PACS: 06.30.Ft, 07.77.Gx, 32.10.–f

DOI: 10.1088/1674-1056/ac8344

1. Introduction

During the movement of atoms in a magnetic field, when the change rate of the magnetic field experienced by an atom is higher than the Larmor procession frequency the atomic magnetic moment fails to follow the magnetic field at such a rapid rate. Thus, atomic non-adiabatic transitions occur between the Zeeman sublevels; these are called Majorana transitions.[1] In a thermal beam clock, the Majorana transition frequency shift is significant owing to the existence of strong magnetic fields and atoms moving at high speed.[2–4] By contrast, the Majorana transition frequency shift is relatively small in a caesium atomic fountain clock because of the weak magnetic field and slow atomic velocity.[5–8] However, once the magnetic field design is no longer perfect, with a large gradient and near-zero magnetic field at the entrance of the magnetic shielding, Majorana transitions, and the problems associated with this phenomenon in experiments, will occur.[9,10] In this study, the Majorana transition frequency shift of a caesium atomic fountain clock was investigated, and its mechanism was theoretically analyzed. The frequency shifts of different initial atomic states in different axial magnetic fields were numerically simulated using the Monte Carlo method. Moreover, a dual-frequency state selection experiment was designed to prepare the asymmetrically populated atoms. Subsequently, the Majorana transition frequency shift of two groups of initial antisymmetrically populated atoms was measured, and the relationship between the Majorana transition frequency shift and axial magnetic field was derived. Based on the measurement results, the magnetic field was optimized to avoid the occurrence of Majorana transition and reduce the frequency shift.

2. Mechanism of the Majorana transition frequency shift in caesium atomic fountain clocks

A schematic of a caesium atomic fountain clock is shown in Fig. 1. First, magneto-optical trap technology was applied to capture and cool the atoms, then the gradient magnetic field produced by anti-Helmholtz coils was switched off to form a cold atomic cloud. After releasing the cold atomic cloud for 30 ms–50 ms, the upward and downward cooling beams were detuned to launch the cold atomic cloud upward. Next, the temperature of the cold atomic cloud was further reduced to 7.5 μK after polarization gradient cooling.[11] The prepared cold atoms were uniformly distributed on the nine Zeeman sublevels of $F = 4$. After entering the state selection cavity, the transitions $|4,0\rangle \rightarrow |3,0\rangle$ occurred in the microwave

†Corresponding author. E-mail: wangxl@ntsc.ac.cn

© 2023 Chinese Physical Society and IOP Publishing Ltd

magnetic field, and the residual atoms in state $|4\rangle$ were eliminated by pushing laser light. The cold atomic cloud passed through Ramsey cavity twice during its upward and downward movements, and Ramsey transition occurred. Both the Ramsey cavity and the atomic free flight region were placed inside four-layer magnetic shielding. A weak 160 nT magnetic field was generated by the C-field coil inside the magnetic shielding, which was used to provide a quantized axis for atomic transitions and remove degeneracy.[12] A magnetic field compensation coil was placed at the lower opening end of magnetic shielding to adjust the intensity and gradient of the magnetic field. Thus, the Majorana transition could be inhibited or eliminated.[13,14] The fall of the cold atomic cloud was monitored by a dual-energy-level fluorescence detection system for normalized detection. According to the normalized Ramsey transition signal, a microwave signal consistent with the clock transition $|3,0\rangle \rightarrow |4,0\rangle$ was constantly output by the servo-controlled frequency synthesizer.

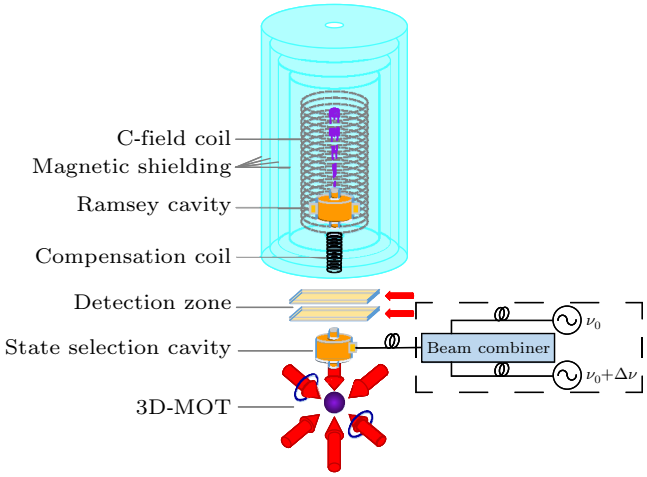


Fig. 1. Schematic of a caesium atomic fountain clock.

When a cold atomic cloud passed through the entrance of the magnetic shielding, the magnetic field decreased rapidly from 10^4 nT to nearly 0 nT within a range of 10 cm, and the atomic velocity was approximately 3.3 m·s^{-1}. If the rate of change of the magnetic field is higher than the Larmor precession frequency, the atomic magnetic moment cannot follow the changing magnetic field. Thus, this may cause the upward-flying caesium atoms to transit from the state $|3,0\rangle$ non-adiabatically to the coherent superposition states of $|3,m'_F\rangle$ ($m'_F = -3,\ -2,\ -1,\ \ldots,\ 3$), and the Majorana transition occurs, as shown in Majorana region I in Fig. 2. The atoms keep flying up and down, passing through Ramsey cavity twice and interacting with the magnetic field. Because the cold atomic cloud has a certain volume and temperature, and the microwave magnetic field in a Ramsey cavity has a radial component,[15] $\Delta F = 1$, $\Delta m_F = \pm 1$ Ramsey transitions would occur besides the clock transition.[16,17] As demonstrated in Ramsey regions I and II in Fig. 2, the black lines represent the transitions $|3,0\rangle \rightarrow |4,\pm 1\rangle$ and the red lines represent the transitions $|3,\pm 1\rangle \rightarrow |4,0\rangle$. Because the atomic population in states $|3,m'_F\rangle (m'_F = \pm 2,\pm 3)$ is small and these energy levels are far away from $|3,0\rangle$, only the atoms in state $|3,0\rangle$ and its adjacent states $|3,\pm 1\rangle$ are considered here. After Ramsey transition, the cold atomic cloud in the superposition states $|4,0\rangle$ and $|4,\pm 1\rangle$ keep falling down, passing through the entrance of the magnetic shielding and experiencing Majorana transition again. Finally, the caesium atoms would eventually transit non-adiabatically to the superposition states of all the Zeeman sublevels. In summary, Majorana transition frequency shift occurs when the atomic states coupled with adjacent energy levels through Majorana transition are affected by Ramsey frequency pulling,[18] thus inducing a clock transition frequency shift.

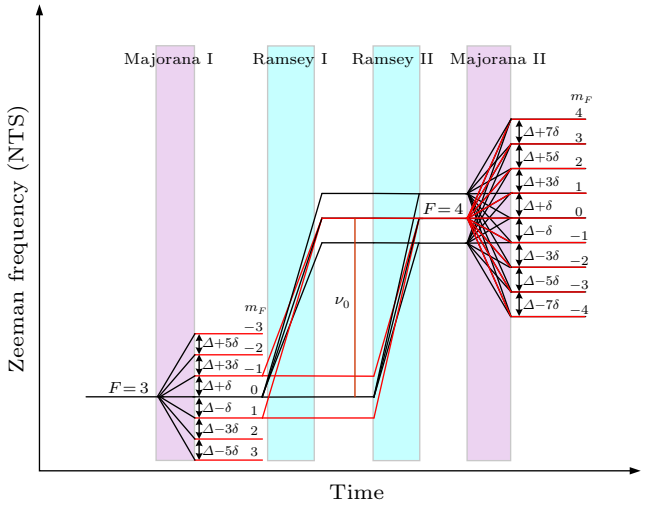


Fig. 2. Hyperfine energy levels of caesium atom in the ground state.

According to Ref. [19], atomic adiabatic transition requires that the magnetic field intensity B and gradient $\partial \boldsymbol{B}/\partial z$ meet the following condition:

$$\frac{1}{B}\left|\frac{\partial \boldsymbol{B}}{\partial z}\right| v\sin\Theta \ll \frac{\mu_{\mathrm{B}} B(g_J - g_I)}{(2I+1)\hbar}, \tag{1}$$

where g_J and g_I are the electronic and nuclear g factors, respectively. μ_{B} is Bohr's magneton, $\hbar$ is the reduced Planck constant, $v = 3.3$ m·s^{-1} is the atomic velocity, I is the nuclear spin angular momentum quantum number and Θ is the angle between the vectors $\boldsymbol{B}$ and $\partial \boldsymbol{B}/\partial z$. Based on calculation, we concluded that the Majorana atomic transition could be avoided if the magnetic field intensity B in the range of 1 cm is greater than 30 nT and the gradient $\partial \boldsymbol{B}/\partial z$ is less than 50 nT·cm^{-1}.

When a caesium atom in state $|F,m_F\rangle$ passes through a weak and static magnetic field with a large gradient, the probability of transition to the state $|F,m'_F\rangle$ at moment t is expressed by the Majorana transition equation as follows:[1]

$$P_{m_F,m'_F} = (F+m_F)!(F-m_F)!(F+m'_F)!(F-m'_F)! \times \cos^{4F}\frac{\beta}{2}\left[\sum_r \frac{(-1)^r(\tan\frac{\beta}{2})^{m'_F-m_F+2r}}{r!(F+m_F-r)!(m'_F-m_F+r)!(F-m'_F-r)!}\right]^2, \quad (2)$$

where $\sum$ denotes the sum of all integers r that ensures the factorial terms are non-negative.

The Majorana transition probability for two-energy-level atoms with the same gyromagnetic ratio in the same magnetic field is expressed as follows:

$$\sin^2\frac{\beta}{2} = P_{\frac{1}{2},-\frac{1}{2}} = \mathrm{e}^{-(\gamma^2B^2/\omega')\pi/2}, \quad (3)$$

where ω' represents the rate of change of the radial magnetic field against time, γ is the gyromagnetic ratio and B is the axial magnetic field intensity, which determines the atomic transition frequency between the Zeeman levels. A weak axial magnetic field and a radial magnetic field that changes rapidly increase the Majorana transition probability. However, a strong axial magnetic field and a slowly varying radial magnetic field can inhibit the Majorana atomic transition.

Moreover, the Majorana transition probability is symmetrical, as expressed in the following equation:

$$P_{m_F,m'_F} = P_{m'_F,m_F} = P_{-m_F,-m'_F}. \quad (4)$$

According to the Breit–Rabi equation,[20] for caesium atoms in a magnetic field $\boldsymbol{B}$, the frequency difference between the two adjacent Zeeman sublevels of the energy level F, $m_F = m_1$ for the low energy state and $m_F = m_2$ for the high energy state, is expressed as follows:

$$\Delta\nu_{m_2-m_1} = \Delta \pm (2m_1 \pm 1)\,\delta, \quad (5)$$

where '$-$' applies when $F = 3$, $\Delta = 3.5098B \times 10^9$ Hz·T^{-1} and $\delta = 1.3358 \times 10^9 B^2$ Hz·T^{-2} and '$+$' applies when $F = 4$, $\Delta = 3.4986B \times 10^9$ Hz·T^{-1} and $\delta = -1.3358 \times 10^9 B^2$ Hz·T^{-2}, as shown in Fig. 2. In a low-frequency magnetic field, the atoms only perform coherent transitions between Zeeman sublevels $F = 3$ or 4.

A weak magnetic field with a large gradient acting on a moving atom can be considered as a low-frequency magnetic field acting on a stationary atom.[21] The low-frequency magnetic field is on the x-axis perpendicular to the C-field, expressed as $B_{\mathrm{L}}(t) = B_{\mathrm{L}0}\cos(2\pi\nu t + \varphi)$, where $B_{\mathrm{L}0}$, $2\pi\nu$, and φ represent the amplitude, angular frequency and initial phase, respectively. Considering the combined influence of the low-frequency magnetic field and the axial C-field $\boldsymbol{B}$, the Hamiltonian operator of an atom is expressed as $\boldsymbol{H}_{\mathrm{L}} = \mu_{\mathrm{B}}(B_{\mathrm{L}}\boldsymbol{i} + B\boldsymbol{k})(g_I I + g_J J)$. The atomic state wave function $|\Psi\rangle$ satisfies the Schrödinger equation as follows:

$$\boldsymbol{H}_{\mathrm{L}}|\Psi\rangle = \mathrm{i}\hbar\frac{\partial}{\partial t}|\Psi\rangle. \quad (6)$$

In a seven-level atomic system $|3, m_F\rangle (m_F = 3, 2, 1, \ldots, -3)$, the time-dependent Hamiltonian $\boldsymbol{H}_{\mathrm{L}}$ is transformed unitarily into $\boldsymbol{H}'_{\mathrm{L}}$ with no apparent time t.[19] In this representation, the matrix elements of the unitary transformation operator U are expressed as follows:

$$\langle F, m_2|U|F, m_1\rangle = \delta_{m_1 m_2}\,\mathrm{e}^{-\mathrm{i}(E_0/\hbar - 2\pi m_1\nu)t}, \quad (7)$$

where $\delta_{m_1 m_2}$ is the Kronecker function. Assuming that each component of the atomic state wave function $|\Psi\rangle$ is expressed as $C_n(t)$, then the wave function after unitary transformation is $|\Psi'\rangle$, whose component is denoted by $A_n(t)$ and satisfies the following relation:

$$A_n(t) = U^*_{nn}C_n(t). \quad (8)$$

Consequently, the matrix expression of the Schrödinger equation (as expressed in Eq. (6)) is given as follows:

$$\mathrm{i}\frac{\partial}{\partial t}\begin{pmatrix} A_1(t)\\ A_2(t)\\ A_3(t)\\ A_4(t)\\ A_5(t)\\ A_6(t)\\ A_7(t)\end{pmatrix} = \begin{pmatrix} 2\pi(3\nu-3\Delta+9\delta) & b_3\mathrm{e}^{\mathrm{i}\varphi}/2 & 0 & 0 & 0 & 0 & 0\\ b_3\mathrm{e}^{-\mathrm{i}\varphi}/2 & 2\pi(2\nu-2\Delta+4\delta) & b_2\mathrm{e}^{\mathrm{i}\varphi}/2 & 0 & 0 & 0 & 0\\ 0 & b_2\mathrm{e}^{-\mathrm{i}\varphi}/2 & 2\pi(\nu-\Delta+\delta) & b_1\mathrm{e}^{\mathrm{i}\varphi}/2 & 0 & 0 & 0\\ 0 & 0 & b_1\mathrm{e}^{-\mathrm{i}\varphi}/2 & 0 & b_1\mathrm{e}^{\mathrm{i}\varphi}/2 & 0 & 0\\ 0 & 0 & 0 & b_1\mathrm{e}^{-\mathrm{i}\varphi}/2 & -2\pi(\nu-\Delta-\delta) & b_2\mathrm{e}^{\mathrm{i}\varphi}/2 & 0\\ 0 & 0 & 0 & 0 & b_2\mathrm{e}^{-\mathrm{i}\varphi}/2 & -2\pi(2\nu-2\Delta-4\delta) & b_2\mathrm{e}^{-\mathrm{i}\varphi}/2\\ 0 & 0 & 0 & 0 & 0 & b_3\mathrm{e}^{-\mathrm{i}\varphi}/2 & -2\pi(3\nu-3\Delta-9\delta)\end{pmatrix}\begin{pmatrix} A_1(t)\\ A_2(t)\\ A_3(t)\\ A_4(t)\\ A_5(t)\\ A_6(t)\\ A_7(t)\end{pmatrix}, \quad (9)$$

where the rotating wave approximation is performed during Hamiltonian unitary transformation and the higher-frequency oscillation terms containing 2ν in the low-frequency transition matrix elements are eliminated; b_j ($j = 1, 2, 3$) denotes the amplitude

of the low-frequency transition matrix elements. The atomic state at any time instant can be determined by solving the Schrödinger equation.

According to the normalization of wave function, we solved the secular equation of the Hamiltonian operator $\boldsymbol{H}'_{\rm L}$ and obtained the j-th eigenvalue λ_j and the corresponding eigenvectors ($D_{(j)1}$, $D_{(j)2}$, $D_{(j)3}$, $D_{(j)4}$, $D_{(j)5}$, $D_{(j)6}$, $D_{(j)7}$), where j is in the range of 1 to 7. According to the matrix characteristics of $\boldsymbol{H}'_{\rm L}$, each component of the eigenvectors can be expressed as follows:

$$D_{(j)n} = D^0_{(j)n}\,\mathrm{e}^{-\mathrm{i}n\varphi}, \tag{10}$$

where $D^0_{(j)n}$ is the n-th component amplitude of the eigenvector or is multiplied by an exponential term.

Therefore, the solution to Eq. (9) can be expressed using the eigenvectors of $\boldsymbol{H}'_{\rm L}$ as follows:

$$A_n(t) = \sum_{j=1}^{7} l_j D^0_{(j)n}\,\mathrm{e}^{-\mathrm{i}n\varphi-\mathrm{i}\lambda_j(t-t_0)/\hbar}, \tag{11}$$

where the coefficient l_j is determined using the initial condition $C_n(t_0)$ of the atom at moment t_0, and the eigenvector's orthonormality, which is expressed as follows:

$$l_j = \sum_{n=1}^{7} {D^0_{(j)n}}^* C_n(t_0)\,\mathrm{e}^{\mathrm{i}n\varphi+\mathrm{i}[E_0/\hbar-2\pi\nu(4-n)]t_0}. \tag{12}$$

Therefore, the Schrödinger equation (Eq. (6)) can be solved by combining Eqs. (8) and (11) as follows:

$$\begin{aligned} C_n(t) \;=\; & \mathrm{e}^{-\mathrm{i}[E_0/\hbar-2\pi\nu(4-n)]t} \\ & \times \sum_{s=1}^{7} C_s(t_0)\,\mathrm{e}^{\mathrm{i}(s-n)\varphi+\mathrm{i}[E_0/\hbar-2\pi\nu(4-s)]t_0} \\ & \times \sum_{j=1}^{7} {D^0_{(j)s}}^* D^0_{(j)n}\,\mathrm{e}^{-\mathrm{i}\lambda_j(t-t_0)/\hbar} \end{aligned} \tag{13}$$

assuming

$$\sum_{j=1}^{7} D^*_{(j)s} D_{(j)n}\,\mathrm{e}^{-\mathrm{i}\lambda_j(t-t_0)/\hbar} \equiv A_{sn}\,\mathrm{e}^{\mathrm{i}\varphi_{sn}}. \tag{14}$$

The atomic state vector component $C_n(t)$ at moment t can be expressed as follows:

$$C_n(t) = U_{nn}(t) \sum_{s=1}^{7} U^*_{ss}(t_0) C_s(t_0) A_{sn}\,\mathrm{e}^{\mathrm{i}\varphi_{sn}}, \tag{15}$$

where A_{sn} and φ_{sn} denote the contribution of the amplitude and phase from the s-th to the n-th atomic state vector component during the Majorana transition. Thus, an analytical expression of the atomic state after the Majorana transition including both the amplitude and phase information is obtained.

Because the cold atom cloud has a certain temperature and volume, it undergoes free expansion during the rising and falling stages. Therefore, the radial microwave magnetic field of the TE_{011} mode in the Ramsey cavity also participates in the Ramsey transition. Furthermore, some atoms at the edge are intercepted by the cut-off waveguide (with a radius of 6 mm) of the Ramsey cavity and therefore cannot arrive at the detection region. As in the calculation of the Majorana atomic transition, the atomic state after the Majorana transition is considered as the initial state. By solving the Schrödinger equation of the atom under the joint effect of the C-field and high-frequency microwave magnetic field, the atomic state after the Majorana transition and Ramsey frequency pulling can be obtained, and the final clock transition signal P can then be derived. The frequency shift of the clock transition caused by the Majorana transition is expressed as δ', and the clock transition signal P near the resonant frequency ν_0 is expressed as follows:

$$P = \sin^2 2bT \cos^2[\pi\tau(\Delta' - \delta')], \tag{16}$$

where the Rabi frequency b is the amplitude of the clock transition matrix element, T denotes atomic free evolution time between the two Ramsey interactions, τ is the single action time of the microwave on the atom and Δ' describes the frequency detuning of the microwave relative to clock transition. Because the linewidth of the Ramsey transition spectrum is 1 Hz, δ' is expressed as follows:

$$\delta' = (P_{1/2} - P_{-1/2})/[2\pi T(P_0 - P_1)], \tag{17}$$

where $P_{1/2}$, $P_{-1/2}$, P_0, and P_1 represent the atomic transition probabilities when the frequency detuning values of the microwave with respect to clock transition are 0.5 Hz, −0.5 Hz, 0 Hz, and 1 Hz, respectively.

Equation (16) is used to calculate the single Majorana transition frequency shift δ' in a static state. If there is no Majorana transition frequency shift $P_{1/2} = P_{-1/2}$. However, if this frequency shift occurs $P_{1/2} \neq P_{-1/2}$, and the magnitude of this frequency shift is calculated using Eq. (17) directly without frequency feedback. Once the feedback of the clock transition frequency comes into play, the frequency shift δ' is reduced to the microwave frequency, and therefore $P_{1/2}$ is equal to $P_{-1/2}$ dynamically and $\delta' = 0$.

After leaving Ramsey cavity, the atomic cloud passes through the entrance of the magnetic shielding for the second time, and the Majorana transition recurs. However, because the laser detection system cannot distinguish the magneton energy levels in state $|4, m_F\rangle$, the Majorana transitions between Zeeman sublevels in state $|4, m_F\rangle$ do not affect the clock transition frequency.

3. Numerical simulation of the Majorana transition frequency shift

According to theoretical analysis presented in Section 2, the exact distribution of the magnetic field at the entrance of the magnetic shielding is essential for calculating the Majorana transition frequency shift. By setting the central vertex of the Ramsey cavity as the reference point, and assuming the upward direction to be the positive direction of the z-axis, we used finite element analysis to simulate the axial and radial magnetic fields along the z-axis.[22] The C-field coil was spirally wound with 97 double-wire turns of diameter 260 mm, height 730 mm and current 1007 μA. Then it was placed in the magnetic shielding comprising four permalloy tubes. The compensation coil had a total of 25 turns, a diameter of 50 mm and a height of 110 mm and was located at the opening of the lower end of the magnetic shielding. The simulation results for the magnetic field are indicated by the three curves in Fig. 3, with Figs. 3(a) and 3(b) representing the axial and radial magnetic field distribution along the z-axis, respectively. The black, blue and red lines correspond to the three typical compensation currents as $I_1 = 0$ μA, 70 μA, and 220 μA, respectively. The change in magnetic field distribution is a result of the combined effect of the compensation current and magnetic shielding. Three end-caps were present, spaced 3 cm apart at the entrance to the magnetic shielding. The thickness of each end-cap was 2 mm, and the magnetic permeability of the magnetic shielding was significantly high. Thus, the simulated magnetic field varied greatly near each end-cap. No zero-crossing point was observed in the axial magnetic field. Around a height of −20.5 cm the axial magnetic field was weak, whereas the radial magnetic field gradient was large. As the compensation current was gradually reduced, the radial magnetic field remained unchanged, whereas the axial magnetic field weakened accordingly and its gradient became larger. When the compensation current was 0, the axial magnetic field near a height of −20.5 cm was reduced to 30 nT and the magnetic field gradient was 60.4 nT·cm^{-1}. Thus, atoms were more prone to Majorana transitions when they passed through this region at a high velocity.

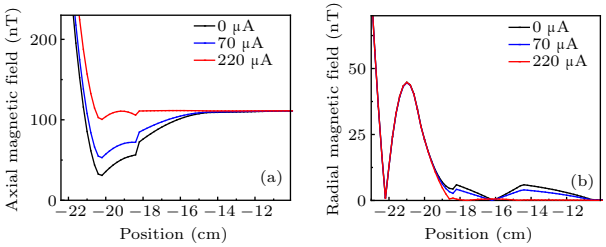


Fig. 3. Distribution of the magnetic field along the z-axis at the entrance to the magnetic shielding of the caesium atomic fountain clock: (a) axial; (b) radial.

According to the simulated results for the magnetic field, we developed interpolation functions to replace the axial static magnetic field B and the radial low-frequency field $B_{\rm L}$ in the Schrödinger equation (as expressed in Eq. (9)). The atomic state information after the Majorana transition was obtained by solving this equation. By setting this atomic state as the initial state for Ramsey transition, and using the Monte Carlo method to simulate the temperature and position of the cold atomic cloud that satisfied the Maxwell and Gaussian distribution, respectively,[23] we solved the Schrödinger equation in the regime of the high-frequency magnetic field. Subsequently, the final atomic state and the corresponding clock transition signal P were determined. Based on the Majorana transition frequency shift equation (as expressed in Eq. (17)), the actual frequency shift was determined.

The initial atomic population and the magnetic field at the entrance to the magnetic shielding (compensation coil current) are two important factors that determine the Majorana transition frequency shift. With the same initial atomic population, the lower the compensation current is the higher the Majorana atomic transition probability. When three sets of compensation currents $I_1 = 42.7$ μA, 58.8 μA, and 67.2 μA were configured and the initial state atoms were only populated in states $|3,0\rangle$ and $|3,-1\rangle$, the relationship between the Majorana transition frequency shift and N_{-1} the population of atoms in the state $|3,-1\rangle$ was calculated, and was found to be a quadratic function, as shown in Fig. 4(a).

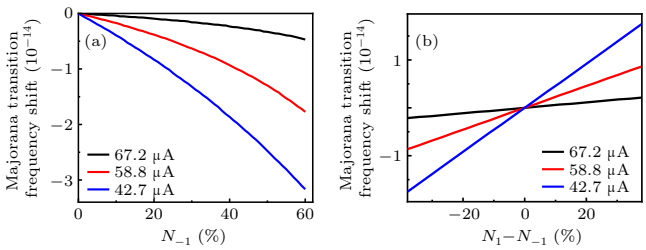


Fig. 4. Relationship between Majorana transition frequency shift and the initial atomic state: (a) atomic population in state $|3,-1\rangle$; (b) atomic population difference in states $|3,\pm1\rangle$.

The same compensation currents were configured with $I_1 = 42.7$ μA, 58.8 μA, and 67.2 μA, and the atoms of the initial state were populated in three states, $|3,0\rangle$ and $|3,\pm1\rangle$, with the atomic population in state $|3,0\rangle$ being a constant $N_0 = 62\%$. The relationship between the Majorana transition frequency shift and $N_1 - N_{-1}$ (the difference in the atomic population of atoms in the two states $|3,\pm1\rangle$) was calculated and was found to be linear and symmetrical with respect to the origin, as shown in Fig. 4(b).

According to the above simulation results, the following two requirements must be met to realize the measurement of the Majorana transition frequency shift: (i) the frequency shift must be large enough to be measured, and therefore asymmetric populated atoms are required; (ii) the symmetry of atomic population cannot be too low, because the loss of symmetry

will reduce the stability of the atomic fountain clock, resulting in a longer measurement period of this frequency shift. Simultaneously, the frequency drift caused by the frequency reference (hydrogen maser) will bring a measurement error to this frequency shift.

We set the initial atomic population in states $|3,0\rangle$ and $|3,-1\rangle$ as follows: $N_0 = 62\%$ and $N_{-1} = 38\%$, which satisfied these two requirements simultaneously. This frequency shift was amplified to the order of 10^{-14} and its measurement uncertainty was kept less than 2×10^{-15}. The relationship between the Majorana transition frequency shift and compensation current was calculated, as shown in Fig. 5. With an increase in current, the frequency shift exhibited a tendency to transform from random to regular oscillations. When the current was below 70 μA, the Majorana transition was the most apparent, and the maximum frequency shift was 3×10^{-14}. When the current exceeded 200 μA, the frequency shift oscillated periodically with a period of 78 μA. When the compensation current increased, the axial magnetic field proportionally increased. Therefore, with an increase in the compensation current, the Majorana atomic transition probability gradually decreased with the coherent phase between the atomic states proportionally increased. The periodic oscillation meant that the Majorana transition frequency shift was largely, but not completely, inhibited, and the changes in current mainly affected the phase of the atomic state.[18,24] Only if the current increases to a certain value can the magnetic field satisfy the atomic adiabatic transition condition and the frequency shift vanish. However, the current should not be too high as this would change the magnitude of the second-order Zeeman frequency shift.

During normal operation of the caesium atomic fountain clock, the frequency shift was reduced by two orders of magnitude and the period remained unchanged. So the compensation current value for normal operation can be set to the zero-frequency-shift point near 200 μA in Fig. 5.

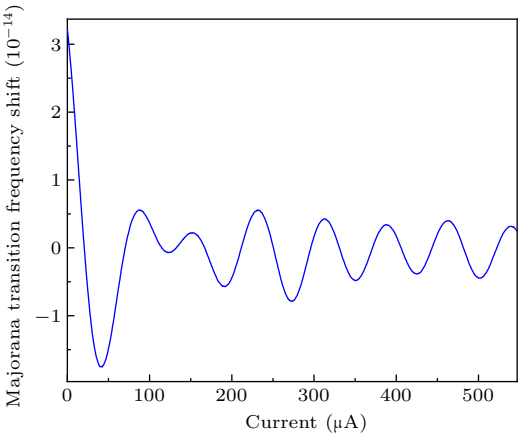


Fig. 5. Relationship between the Majorana transition frequency shift and the compensation current.

4. Experimental analysis of Majorana transition frequency shift

The numerical simulations introduced in Section 3 indicate that the Majorana transition frequency shift is determined by the population of the initial atomic state as well as the magnetic field along the atomic trajectory. When the fountain clock is operating normally, the atoms in the initial state demonstrate a high level of symmetry after state selection, with almost all of them in state $|3,0\rangle$. In this experiment, the atomic population at each Zeeman sublevel of $F = 3$ after the Majorana transition was measured under different compensation currents. When the atoms moved upward through the Ramsey cavity, a single pulse microwave was fed to excite the atoms to perform a Rabi transition ($\Delta F = 1$, $\Delta m_F = 0$). By varying the microwave frequency, time-of-flight signals were collected and the population of atoms after the Majorana transition in each Zeeman sublevel was obtained. According to Eqs. (1) and (2), we obtained the measured and fitted results shown in Fig. 6. The horizontal axis represents the compensation current and the vertical axis represents the atomic population. Figure 6(a) shows the measured value and fitted curve of the atomic population in state $|3,0\rangle$. With a reduction in the current, the atomic population in this state rapidly decreased, and the atoms transited to other Zeeman sublevels. Figure 6(b) shows the atomic population in states $|3,\pm1\rangle$ and $|3,\pm2\rangle$. With a reduction in the current, the atomic population in states $|3,\pm1\rangle$ rapidly increased because they are close to state $|3,0\rangle$. When the current was reduced to 20 μA, the atomic population in states $|3,\pm1\rangle$ increased to its maximum, and began to transit to states $|3,\pm2\rangle$ in large quantities. At this moment, the number of atoms in state $|3,0\rangle$ was similar to that in states $|3,\pm1\rangle$, and remained unchanged. Because of the large energy interval between states $|3,\pm3\rangle$ and $|3,0\rangle$, the Majorana transition probability was low. In the experiment, the atoms in the states $|3,\pm3\rangle$ were not observed.

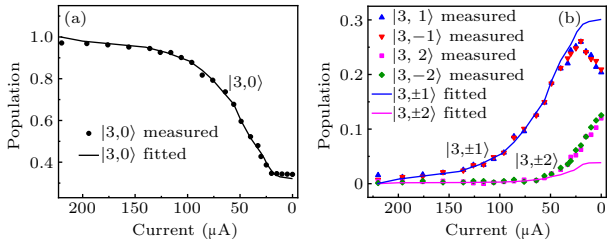


Fig. 6. Relationship between the current and atomic population after Majorana transition during normal operation of a caesium atomic fountain clock.

The simulation results indicated that when the initial atoms were symmetrically populated the Majorana transition frequency shifts would cancel each other. When the caesium atomic fountain clock was in normal operation, almost all atoms after state selection were in the single state $|3,0\rangle$.

Even though these atoms performed Majorana transitions, the atomic population was still highly symmetrical. During its normal operation, the Majorana transition frequency shift is significantly small, hence it cannot be measured in an experiment. Therefore, the initial asymmetric populated atoms are required to amplify this frequency shift.[25]

The experimental device used in this study is indicated by a dotted box in Fig. 1. Two microwave signal sources of model SMB100A produced by R&S (Rohde & Schwarz, Germany) were used for the dual-frequency state selection, and both signal sources were referenced to the same hydrogen maser (VCH-1003M). The microwave signals of different frequencies generated by the two sources passed through the beam combiner and were fed simultaneously into the state selection cavity. After state selection, the atoms were asymmetrically populated at the two sublevels of $F = 3$, indicating that the initial asymmetric populated atoms were prepared. In the first group of experiments, the frequency and power of the two state-selective microwave signals were 9192631813 Hz, -51.6 dBm and 9192409000 Hz, -30.6 dBm, respectively, which corresponded to the ground state transitions $|4,0\rangle \rightarrow |3,0\rangle$ and $|4,-1\rangle \rightarrow |3,-1\rangle$ of caesium atoms. The current of the compensation coil was set to 220 μA, whereas other parameters of the fountain clock remained unchanged. The atomic population in each sublevel was measured; these were $N_0 = 62\%$ for the atoms in state $|3,0\rangle$ and $N_{-1} = 38\%$ for the atoms in state $|3,-1\rangle$. When the current of the compensation coil was gradually reduced, the atomic population in each Zeeman sublevel was then measured, as shown in Fig. 7.

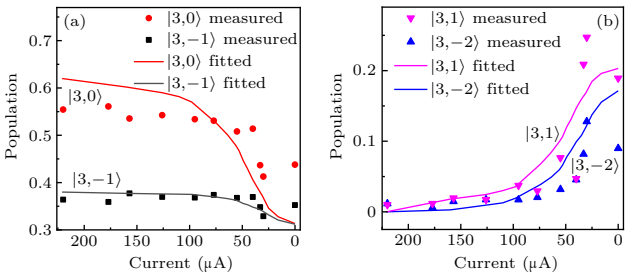


Fig. 7. Relationship between the current and atomic population after Majorana transition with the initial atoms populated asymmetrically.

Figure 7(a) displays the measured atomic population in states $|3,0\rangle$ and $|3,-1\rangle$ and figure 7(b) displays those of states $|3,1\rangle$ and $|3,-2\rangle$. When the current was reduced, the atomic population in states $|3,0\rangle$ and $|3,-1\rangle$ decreased whereas that in states $|3,1\rangle$ and $|3,-2\rangle$ increased. Initially, there are 20% more atoms in state $|3,0\rangle$ than in state $|3,-1\rangle$. Thus, a higher atomic transition was observed from state $|3,0\rangle$ to state $|3,-1\rangle$ compared with the atomic transition from state $|3,-1\rangle$ to state $|3,0\rangle$, indicating that the reduction in speed for the atoms in state $|3,0\rangle$ was more significant compared with those in $|3,-1\rangle$. Furthermore, an increase in speed for atoms in state $|3,1\rangle$, being close the state $|3,0\rangle$, was more significant than that of atoms in state $|3,-2\rangle$. The measured results illustrated in Figs. 6 and 7 prove that the atomic population in each state varies significantly, and the Majorana atomic transition is noticeable when the current is below 90 μA. For the fluctuations in laser power, atomic population and magnetic field, and because the Majorana atomic transition probability is more sensitive to weak magnetic fields, the deviation between the fitted and measured results is quite large.

Taking a hydrogen maser (with a frequency drift rate of 7×10^{-17} day^{-1}) as the frequency reference, with the compensation current gradually increasing to 220 μA in steps of 20 μA, the clock frequency under each compensation current was continuously measured for 2 days. At the end of the measurement, the clock was switched back to its normal operational mode and the corresponding clock frequency was measured. The difference between these two frequencies was considered to be the Majorana transition frequency shift, and the results are shown in Fig. 8(a). The frequency shift oscillated as the current increased. When the current was below 90 μA, the effect of Majorana transition was found to be most significant, and the maximum frequency shift reached 2×10^{-14}. The main reasons for the noticeable difference between theoretical calculations and the experimental results at low current are: (i) the magnetic field values substituted in the calculation were obtained via simulation and deviated from the actual magnetic field values to a certain extent; (ii) when the current was low, the magnetic field intensity was near zero with a large gradient. Atoms were more prone to a Majorana transition, and the frequency shift was more sensitive to current change. When the current was above 90 μA, the Majorana atomic transition was inhibited and the atomic phase linearly increased with the current, resulting in this frequency shift periodically changing between $\pm 1 \times 10^{-14}$ and the period was approximately 80 μA. The magnitude, period and tendency of the frequency shift were essentially consistent with the results obtained via calculation in Section 3, which validated the theoretical model.

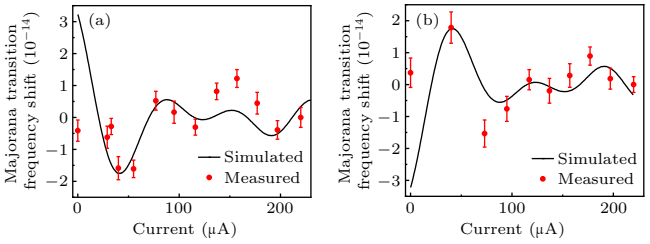


Fig. 8. Relationship between Majorana transition frequency shift and the current of two groups of initial atoms with reverse asymmetric populations.

In the second group of experiments, the same method was used to prepare the atoms, with $N_0 = 62\%$ for the atoms in the state $|3,0\rangle$ and $N_1 = 38\%$ for the atoms in state $|3,1\rangle$. As the

compensation current was gradually increased, Majorana transition frequency shifts were measured under different current values, as shown in Fig. 8(b). The opposite trend was observed in the results in the second group of experiments compared with the first group of experiments. In addition, the results from this group of experiments conformed the simulation results. When the compensation current was 220 μA, the Majorana transition frequency shift was near the zero point. Therefore, this current value was regarded as the optimal value for the fountain clock during its normal operation.

During the aforementioned experiments, the maximum current applied to the compensation coil was 220 μA. This is because an excessive compensating magnetic field may lead to changes in the second-order Zeeman frequency shift,[26] resulting in deviations in the measured Majorana transition frequency shift. In the experiment, we discovered that a compensation current of 220 μA led to a frequency shift of 0.6 Hz in the magnetically sensitive transition of the caesium atoms, and the resulting second-order Zeeman frequency shift was measured to be 0.87×10^{-16}.[12] During normal operation of the caesium atomic fountain clock, the Rabi transition signal was excited and measured and the atomic populations in states $|3,1\rangle$ and $|3,-1\rangle$ were found to be $N_1 = 0.93\%$ and $N_{-1} = 1.01\%$, respectively. Therefore, the Majorana transition frequency shift of the caesium atomic fountain clock was 4.57×10^{-18}.

5. Conclusion

Majorana transition is defined as the non-adiabatic transition between the Zeeman sublevels when the atoms pass through the near-zero magnetic field with a large gradient, resulting in a frequency shift due to the Ramsey frequency pulling effect. By understanding Majorana transition we can help improve the signal-to-noise ratio of atomic fountain clocks and magnetic systems by optimizing the structure of the magnetic shielding and reducing frequency uncertainties. In this study, a physical model was constructed to examine the mechanism of the Majorana transition frequency shift. The relationships among the frequency shift, magnetic field and initial atomic population were investigated via numerical simulations. Finally, the frequency shift was measured with the atoms in asymmetric initial states, which were prepared using dual-frequency state selection technology. The results from the experiments were consistent with the theoretical results from simulations. The compensation current of the fountain clock during normal operation was configured to be 220 μA, and the Majorana transition frequency shift was evaluated to be 4.57×10^{-18}.

Acknowledgments

Project supported by the National Natural Science Foundation of China (Grant No. 12173044), Research and Development Project of Scientific Research Instruments and Equipment of Chinese Academy of Sciences (Grant No. YJKYYQ20200020), Large Research Infrastructures Improvement Funds of Chinese Academy of Sciences (Grant No. DSS-WXGZ-2020-0005), and Chinese Academy of Sciences for Western Young Scholars (Grant Nos. XAB2018A06, XAB2019A07, and XAB2018B16).

References

[1] Majorana E 1932 *Il Nuovo Cimento* **9** 335
[2] Urabe S, Nakagiri K, Ohta Y, Kobayashi M and Saburi Y 1980 *IEEE Trans. Instrum. Meas.* **29** 304
[3] Becker G 1978 *IEEE Trans. Instrum. Meas.* **27** 319
[4] Wang Y Q 1981 *Acta Metrologica Sin.* **2** 42
[5] Du Y B, Wei R, Dong R C and Wang Y Z 2013 **245** 419
[6] Dai S Y, Zheng F S, Liu K, Chen W L, Lin Y G, Li T C and Fang F 2021 *Chin. Phys. B* **30** 013701
[7] Weyers S, Gerginov V, Kazda M, Rahm J, Lipphardt B, Dobrev G and Gibble K 2018 *Metrologia* **55** 789
[8] BIPM https://webtai.bipm.org/ftp/pub/tai/data/PSFS_reports/nrc-fcs2_59609-59634.pdf
[9] Wynands R, Schröder R and Weyers S 2006 *European Frequency and Time Forum*, 2006, Braunschweig, pp. 219–223
[10] Wynands R, Schröder R and Weyers S 2007 *IEEE Trans. Instrum. Meas.* **56** 660
[11] Shi J R, Wang X L, Guan Y, Ruan J, Liu D D, Bai Y, Yang F, Zhang H, Yu F X and Zhang S G 2019 *Acta Phys. Sin.* **68** 190601 (in Chinese)
[12] Shi J R, Wang X L, Bai Y, Yang F, Guan Y, Liu D D, Ruan J and Zhang S G 2021 *Chin. Phys. B* **30** 070601
[13] Gerginov V, Nemitz N, Weyers S, Schröder R, Griebsch D and Wynands R 2010 *Metrologia* **47** 65
[14] Weyers S, Hübner U, Schröder R, Tamm C and Bauch A 2001 *Metrologia* **38** 343
[15] Tsang T 1997 *Classical Electrodynamics* (Washington D.C.: World Scientific Publishing) p. 411
[16] Cutler L S, Flory C A, Giffard R P and De Marchi A 1991 *J. Appl. Phys.* **69** 2780
[17] Bauch A and Schröder R 1993 *Ann. Physik* **505** 421
[18] Gerginov V, Nemitz N and Weyers S 2014 *Phys. Rev. A* **90** 033829
[19] Vanier J and Audoin C 1989 *The Quantum Physics of Atomic Frequency Standards* (Bristol: IOP Publishing)
[20] Ramsey N F 1956 *Molecular Beams* (London: Oxford University Press)
[21] Shirley J H and Jefferts S R 2003 *IEEE International Frequency Control Symposium and PDA Exhibition Jointly with the 17th European Frequency and Time Forum*, May 4–8,2003, Florida, USA, p. 1072
[22] Li R and Gibble K 2004 *Metrologia* **41** 376
[23] Shi J R 2016 *The study of Ramsey and Rabi frequency pulling shift in Cesium fountain clock* (Master Dissertation) (Beijing: University of Chinese Academy of Sciences) (in Chinese)
[24] Lee H S, Kwon T Y, Kang H S, Park Y H, Oh C H, Park S E, Cho H and Minogin V G 2003 *Metrologia* **40** 224
[25] Wynands R and Weyers S 2005 *Metrologia* **42** S64
[26] Li L, Ji J, Ren W, Zhao X, Peng X, Xiang J, Lü D and Liu L 2016 *Chin. Phys. B* **25** 073201